ACS chemical biology

Articles

pubs.acs.org/acschemicalbiology

Metabotyping of the *C. elegans sir-2.1* Mutant Using *in Vivo* Labeling and ^{13}C-Heteronuclear Multidimensional NMR Metabolomics

Yong Jin An,[†,‡] Wen Jun Xu,[†] Xing Jin,[†] He Wen,[†] Hyesook Kim,[§] Junho Lee,[§] and Sunghyouk Park*[,†]

[†]College of Pharmacy, Natural Product Research Institute and [§]WCU Department of Biophysics and Chemical Biology, Seoul National University, Sillim-dong, Gwanak-gu, Seoul, 151-724, Korea

[‡]Department of Biochemistry, College of Medicine, Inha University, Incheon, 400-712, Korea

Supporting Information

ABSTRACT: The roles of *sir-2.1* in *C. elegans* lifespan extension have been subjects of recent public and academic debates. We applied an efficient workflow for *in vivo* ^{13}C-labeling of *C. elegans* and ^{13}C-heteronuclear NMR metabolomics to characterizing the metabolic phenotypes of the *sir-2.1* mutant. Our method delivered sensitivity 2 orders of magnitude higher than that of the unlabeled approach, enabling 2D and 3D NMR experiments. Multivariate analysis of the NMR data showed distinct metabolic profiles of the mutant, represented by increases in glycolysis, nitrogen catabolism, and initial lipolysis. The metabolomic analysis defined the *sir-2.1* mutant metabotype as the decoupling between enhanced catabolic pathways and ATP generation. We also suggest the relationship between the metabotypes, especially the branched chain amino acids, and the roles of *sir-2.1* in the worm lifespan. Our results should contribute to solidifying the roles of *sir-2.1*, and the described workflow can be applied to studying many other proteins in metabolic perspectives.

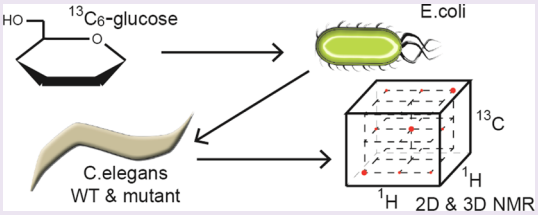

Sirtuins are NAD$^+$-dependent protein deacetylases and have been implicated in lifespan extension for a number of model systems, such as yeasts,[1] nematodes,[2] flies,[3] and mice.[4] They also play important roles in the development of age-related illnesses such as neurodegeneration and cancer in mice[5] and human.[6] These reports generated large public interest, and the development of small molecular mimetics of these proteins has been intensely pursued.[7,8] Among the various sirtuins, *sir-2.1* orthologs (sir2 in yeast and SIRT1 in human) have been studied the most in relation to aging and lifespan. In *C. elegans*, high levels of *sir-2.1* were reported to extend the nematode's lifespan by up to 50%, based on the results from genetically overexpressing strains.[2] In mammalian systems, the orthologous protein SIRT1 has been also shown to have anti-aging effects as well as protective effects against metabolic-syndrome-associated cancers.[9] Recently, however, the genetic approaches used in the original nematode study were challenged, and the life extension was linked to another mutation affecting sensory neurons.[10] Still, *sir-2.1* does seem to contribute to the lifespan extension of *C. elegans*,[11] albeit to a smaller degree (~14%).[11,12] Not only the sirtuins themselves but also the effects of small molecular activators of sirtuins have been a point of debates.[13−15] Therefore, despite the intense academic and public interest, our understanding of this protein's effects is still not sufficient. Especially poorly characterized are its roles in regulating cellular metabolism at individual metabolite levels, even though its effects are essentially related to metabolism and its activity is strongly regulated by small molecular metabolites such as NAD$^+$ or nicotineamide.

Investigating the metabolic effects of genes or gene products may be most relevantly performed by a metabolomics approach, as it can provide direct metabolic signature of biochemical pathways.[16] For the *C. elegans* system, recent NMR metabolomics has provided valuable insights into the metabolic phenotypes (metabotypes) of the animals under various experimental perturbations.[17−19] A limitation of these conventional one-dimensional NMR metabolomics, however, is signal overlap, which can lead to ambiguity in metabolite identification and quantitation.[20] Recent studies addressed these in studying *C. elegans* metabolites by using two-dimensional NMR based on ^{1}H−^{1}H homonuclear correlation.[21−23] However, those still have problems with spectral overlaps involving diagonal peaks and lower sensitivity from small couplings (a few hertz for ^{1}H−^{1}H *versus* ~140 Hz for ^{1}H−^{13}C), and its extension to three-dimensional NMR is impractical. Furthermore, ^{1}H−^{1}H homonuclear correlation may not be enough structural confirmation in many cases, and ^{13}C-heteronuclear multidimensional NMR (^{13}C-HMN) is highly desired. With proper *in vivo* labeling, the ^{13}C-HMN would give highly sensitive and high resolution data, as nicely exemplified for plants, bacteria, silkworm, and mouse systems.[24−26] Still, individual model systems require different *in vivo* labeling schemes, and ^{13}C-HMN has not been applied to metabolomic analysis of *C. elegans* which has been widely used as a model organism in life sciences.

Received: August 13, 2012
Accepted: September 21, 2012
Published: October 8, 2012

Here, we describe a workflow to uniformly label *C. elegans in vivo* with a ^{13}C-stable isotope and to obtain ^{13}C-HMN-based metabolomics data with sensitivity 2 orders of magnitude higher than that of unlabeled samples. The overall strategy allowed the fast acquisition of high resolution two-dimensional (2D) and previously unattainable HCCH-TOCSY three-dimensional (3D) NMR data for *C. elegans* metabolites. We successfully applied the combined techniques to the characterization of the metabotypes of the *C. elegans sir-2.1* knockout (KO) strain. Our results show that the *sir-2.1* KO strain exhibits enhancement in various catabolic pathways, including those of branched chain amino acids, decoupled from ATP production. We propose that these metabolic roles of *sir-2.1* should contribute to the modest lifespan increase caused by *sir-2.1*.

RESULTS

***In Vivo* Metabolic Labeling of *C. elegans*.** As ^{13}C labeling of *C. elegans* can give great advantages in terms of signal resolution and sensitivity in ^{13}C-HMN, we performed *in vivo* metabolic labeling that can label all of the metabolites in *C. elegans* with ^{13}C (Figure 1). The procedure starts with *in vivo*

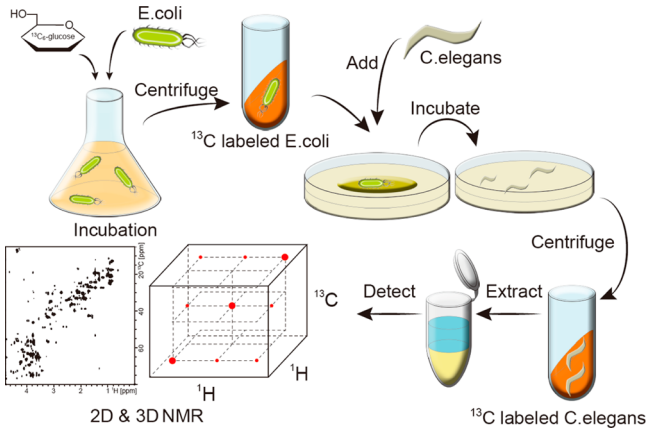

Figure 1. Overall workflow of the study. *E. coli* was labeled with $^{13}C_6$-glucose as a sole carbon source and was fed to *C. elegans*. The worm metabolites were extracted using the double phase extraction method, and the aqueous phase was analyzed with 2D and 3D NMR.

uniform labeling of *E. coli* with $^{13}C_6$-glucose as sole carbon source in M9-based minimal media. This approach has been used in protein NMR community to label recombinant proteins produced in *E. coli*. After harvesting the metabolically labeled *E. coli*, we fed them to *C. elegans* on M9 agar plates, also made with $^{13}C_6$-glucose as sole carbon source. As *E. coli* is preferred food for *C. elegans*, the nematode worms grew normally. Extracts from these *C. elegans* worms were tested for isotopic enrichment with mass spectrometry (Supporting Information, Figure S1). For arginine with a 6-carbon spin system, about 80% of the molecules had six ^{13}C atoms, and 17.4% had five ^{13}C atoms. Overall, over 97% (80% + 17.4%) of the molecules had more than five carbons replaced by ^{13}C isotope. Therefore, the method exhibited efficient incorporation of ^{13}C isotope for multidimensional heteronuclear NMR.

Multidimensional NMR. With the successful labeling, we carried out a 2D ^{13}C-heteronuclear single quantum coherence (HSQC) experiment with the labeled samples from wild type (WT) worms. For comparison, we prepared another sample obtained with exactly the same procedure, but with unlabeled glucose. The obtained spectra showed remarkable difference in terms of detectable peak numbers (Figure 2A and B). The labeled spectrum featured over 300 resolved peaks in just 20 min of data acquisition, while the unlabled one exhibited only a few detectable peaks. Although this high quality two-dimensional NMR is enough for metabolic profiling, confirmation of the identities of marker metabolites requires through-bond connectivity of these signals. In addition, there were still many overlaps in the 2D spectra (Supporting Information, Figure S2). Therefore, we obtained a 3D HCCH-TOCSY spectrum, because it can correlate the entire carbon-connected spin system, greatly assisting the confirmation of the structural identities. The three-dimensional spectrum exhibited excellent signal-to-noise ratio due to the high isotope incorporation (Figure 2C). The spin system identification of metabolites could be achieved for average-sized metabolites, as exemplified by isoleucine with five side chain carbon atoms (Figure 2D). With the help of these multidimensional NMR and databases,[27,28] we identified many more metabolites with confidence than normally observed in one-dimensional NMR (Supporting Information, Table S3).

Multivariate Analysis of 2D NMR Data. Next, we decided to apply the approach to characterizing the metabotypes of *sir-2.1* mutant of *C. elegans* and obtained 2D ^{1}H−^{13}C HSQC spectra for the WT and the knockout mutant. With the recently recognized difficulties in firmly characterizing the overexpressing strain,[10,12] results from the KO strain should be useful in studying this gene. Overall spectral features were quite comparable, consistent with the apparently similar phenotypes (Figure 3A). Still, there were specific differences in peak intensities (Figure 3B), and we applied multivariate data analysis to study these differences holistically over all of the samples.

Orthogonal projections to latent structures-discriminant analysis (OPLS-DA) score plot gave clear discrimination of the two groups with good statistical significance (one predictive component and two orthogonal components, R^2 = 0.817 and Q^2 = 0.855) (Figure 4A), suggesting that these two have readily differentiable metabotypes (see Supporting Information for principal component analysis, Figure S4). Then, we built an S-plot to determine particular peaks responsible for the distinction between WT and *sir-2.1* mutant (Figure 4B). We found that a number of peaks are highly correlated with the different spectral profiles. These results show that WT and *sir-2.1* have distinct metabolite profiles related to particular metabolic pathways.

Differential Metabolites for WT and *sir-2.1* KO. The chemical shift values of the significant signals contributing to the difference were assigned, and their levels were compared (Table 1). The levels of some of the metabolites sharing large common structural motifs (*i.e.*, AMP, ATP, acetyl-CoA, and glutathione disulfide (GSSG)) were also confirmed using a LC−MS approach (Supporting Information, Figure S5). Most of them feature very high significance with their low *p*-values ($\leq 10^{-5}$) from Student's *t* test, showing the robustness of our approach. The overall approach gave a better idea about the identities and significance of the markers that may not be assessed in detail with simple spectral subtraction method (Supporting Information, Figure S6). Many of these, especially branched chain amino acids (BCAAs: leucine, isoleucine, and valine), triacylglycerol and carnitine, acetyl-CoA, elevated in the WT strain, and lactate, alanine, glutamate, fatty acids, and AMP, elevated in the *sir-2.1* mutant, turned out to be involved in cellular energy and redox metabolism. Collectively, the *sir-2.1*

dx.doi.org/10.1021/cb3004226 | *ACS Chem. Biol.* 2012, 7, 2012−2018

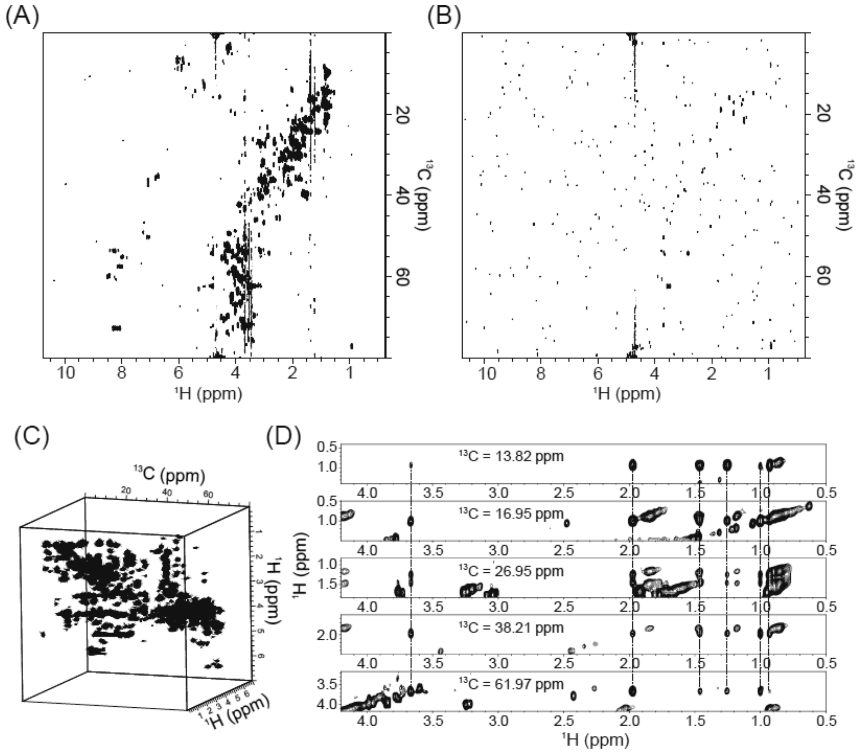

Figure 2. 2D and 3D NMR spectra of whole extracted metabolites from WT *C. elegans*. Representative HSQC NMR spectra (900 MHz) of ^{13}C-labeled (A) and unlabeled (B) samples. (C) 3D cube representation of HCCH-TOCSY spectra for ^{13}C-labeled samples. (D) Strip plot for isoleucine side chain carbon spin systems with each carbon chemical shift.

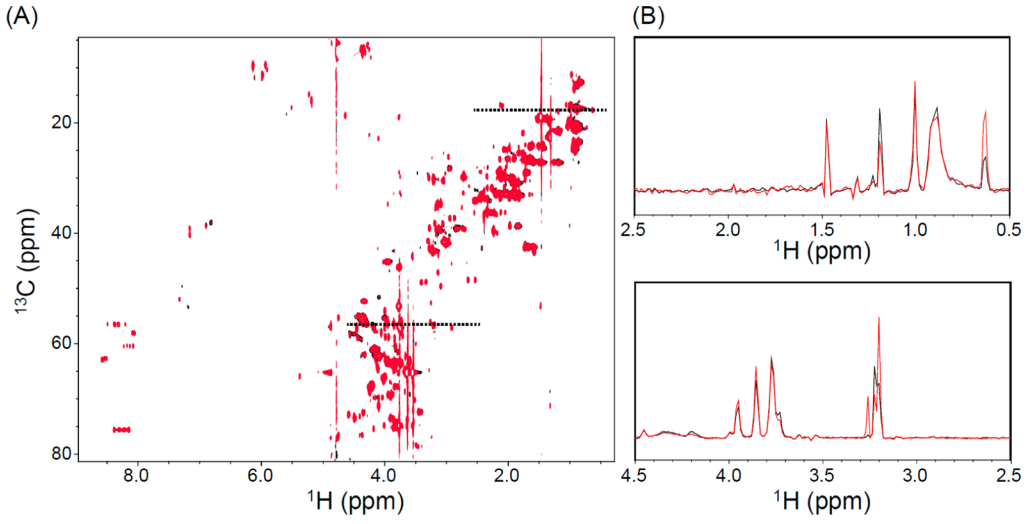

Figure 3. Comparison of HSQC spectra for WT and *sir-2.1* mutant. (A) Spectra for WT (black) and *sir-2.1* mutant (red) are overlaid. Two dotted lines indicate where one-dimensional spectra were extracted for comparison in panel B.

mutants seem to be in lower energy (higher AMP and lower ATP) and higher oxidative status.

DISCUSSION

Our workflow for ^{13}C-HMN-based metabolomics with *C. elegans* has unique technical features over earlier reports. Previous *in vivo* labeling studies of *C. elegans* are designed for mass spectrometry,[29] mostly involving ^{15}N or specific amino acid labeling for proteomic studies.[30−32] ^{13}C-labeling for *C. elegans* optimized for metabolomics with multidimensional NMR has not been reported. In the ^{15}N or amino acid labeling studies, the purposes were to discriminate control and experimental groups by different *m*/*z* values of the same compounds, but our ^{13}C-labeling is for increasing the signal intensities in NMR experiment. Our approach gave sensitivity about 2 orders of magnitude higher than that of unlabeled samples, which allowed the acquisition of fast 2D HSQC and 3D HCCH-TOCSY spectra. For 3D NMR experiments in metabolomics, a ^{13}C−COSY type 3D NMR experiment (HCCH−COSY) has been reported for *Bombyx mori* and *Arabidopsis thaliana*,[24,25] but ^{13}C-TOCSY type 3D (HCCH-TOCSY) experiments have not been used. HCCH-TOCSY can give more information but requires higher isotope incorporation than HCCH−COSY, because the former requires every

dx.doi.org/10.1021/cb3004226 | *ACS Chem. Biol.* 2012, 7, 2012−2018

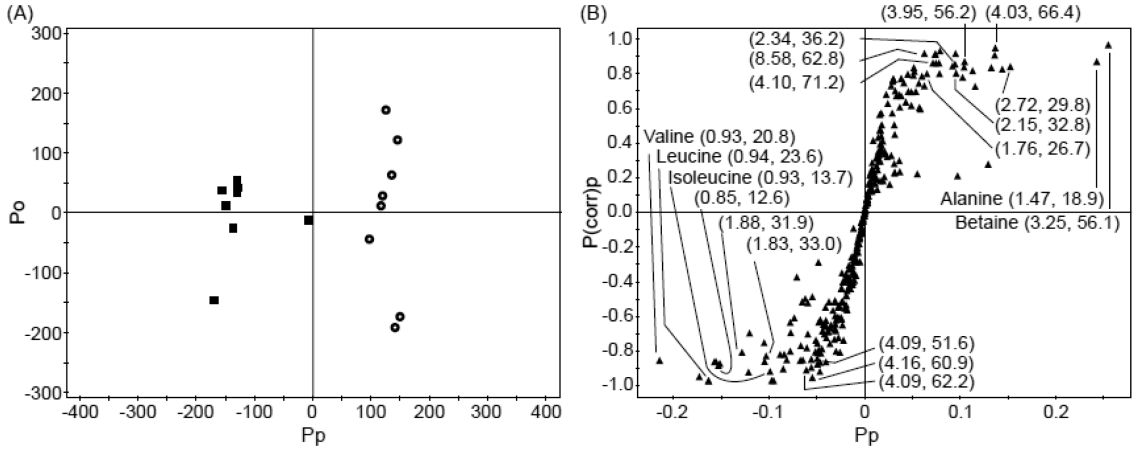

Figure 4. Multivariate analysis between WT and *sir-2.1* mutant data. (A) OPLS-DA score plot showing the different metabolite profiles between WT (filled box) and *sir-2.1* mutant (open circle). (B) S-plot showing the signals contributing to the differentiation. The ^{1}H and ^{13}C ppm values for highly significant contributors are indicated.

Table 1. Levels of Metabolites Contributing to the Difference between WT and *sir-2.1* Mutant

metabolite	change (%)	*p*-value less than	metabolite	change (%)	*p*-value less than
3,7,12α-trihydroxy-5β-cholanate	−39.06 ± 11.20	2.97×10^{-6}	(*S*)-lactate	17.13 ± 6.68	7.87×10^{-5}
carnitine	−40.99 ± 9.53	4.66×10^{-6}	allantoin	47.52 ± 17.07	3.39×10^{-4}
carnosine	−28.80 ± 12.98	3.09×10^{-4}	betaine	633.98 ± 159.12	6.31×10^{-7}
cellobiose	−27.74 ± 8.21	4.23×10^{-6}	choline	97.96 ± 55.07	0.0019
phosphocholine	−34.83 ± 8.53	4.70×10^{-6}	cystathionine	23.76 ± 8.69	4.12×10^{-5}
alanyl-alanine	−43.18 ± 15.22	2.81×10^{-5}	L-alanine	13.39 ± 4.71	2.77×10^{-5}
L-2-aminoadipate	−16.60 ± 6.94	1.55×10^{-6}	L-glutamate	10.16 ± 3.86	6.04×10^{-5}
L-3-amino-isobutanoate	−31.29 ± 11.27	3.52×10^{-5}	L-tryptophan	36.58 ± 18.22	7.25×10^{-4}
L-aspartate	−19.92 ± 9.87	6.94×10^{-4}	shikimate	30.24 ± 15.95	0.0012
L-isoleucine	−19.33 ± 6.40	1.47×10^{-5}	putrescine	32.16 ± 15.32	4.98×10^{-4}
L-leucine	−26.68 ± 6.37	3.49×10^{-7}	fatty acids[a] (acyl chain CH_3)	5.83 ± 2.49	1.88×10^{-4}
L-lysine	−13.25 ± 5.73	7.85×10^{-4}	AMP[b]	39.08 ± 18.75	4.43×10^{-6}
L-methionine	−27.52 ± 10.31	5.26×10^{-5}	glutathione disulfide[b]	10.61 ± 20.42	0.0011
L-valine	−16.45 ± 5.21	8.90×10^{-6}			
N-carbamoyl-L-aspartate	−51.74 ± 35.27	0.0072			
propanoate	−24.49 ± 8.11	1.46×10^{-5}			
triacylglycerol[a] (Glycerol backbone)	−17.72 ± 5.06	2.83×10^{-6}			
ATP[b]	−77.10 ± 19.12	5.53×10^{-7}			
acetyl-CoA[b]	−29.79 ± 27.00	0.0240			

The change values are from area-normalized peak volumes of the 2D-HSQC spectra and represent percent changes of *sir-2.1* with respect to the WT values, with negative values for decrease and positive values for increase. The errors represent the confidence interval at 95% confidence level. [a]Triacylglycerol and fatty acids levels were measured using one-dimensional NMR with organic phase samples. [b]AMP, ATP, glutathione disulfide, and acetyl-CoA have many overlapped peaks, and their levels were confirmed using LC−MS.

carbon in a spin system to be replaced by ^{13}C-isotope, whereas the latter requires only two adjacent carbons in ^{13}C-isotope status. Our HCCH-TOCSY spectrum of isoleucine, an important BCAA with a five carbon branched spin system, exemplifies the efficiency of isotopic labeling and the utility of the spectrum in the identification of the complete carbon spin systems of metabolites.

The metabotyping of *sir-2.1* mutant (Figure 5) serves as a proof of principle of our approach and shows how the overall cell metabolism is modulated in the mutant.

For carbohydrate metabolism, initial glycolytic catabolism seems enhanced on the basis of the higher levels of lactate and alanine, products of pyruvate reduction and transamination, respectively.[33] This is consistent with SIRT1's inactivation of PGAM1,[34] which inhibits glycolysis.[35] However, the downstream TCA cycle seems less active due to the lower levels of BCAAs that fuel the TCA cycle, which leads to lower ATP production. For lipid metabolism, generation of fatty acids is near normal (actually, marginally higher), but the level of the final metabolite, acetyl-CoA, is lower. This can be explained by the lower level of carnitine, a key component of carnitine shuttle required for transporting fatty acids into mitochondria.[36] Therefore, this decreased transport seems to disconnect the initial lipolysis and the β-oxidation, ultimately causing inefficient ATP generation. For nitrogen metabolism, the lower levels of BCAAs and other amino acids (lysine and aspartate) suggest enhanced catabolism. This is supported by the increase in putrescine, generated from amino acid degradation pathway (http://www.genome.jp). Nucleotide nitrogen metabolism also seems shifted toward catabolism, considering that allantoin, a purine catabolism intermediate, is also increased in the mutant.

Normally, catabolism is activated when cellular energy is low, but this compensatory mechanism does not seem to work well in the mutant. As stated above, there is a decoupling between

dx.doi.org/10.1021/cb3004226 | *ACS Chem. Biol.* 2012, 7, 2012−2018

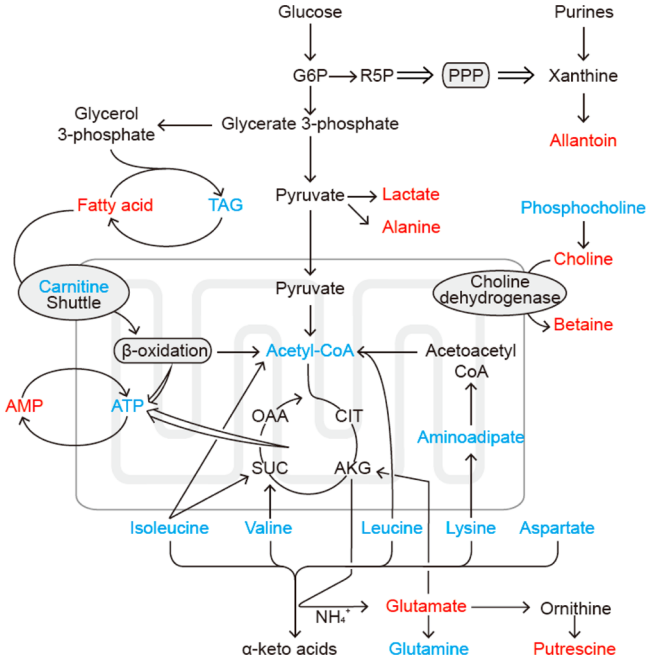

Figure 5. Overall metabotypic characterization of the *sir-2.1* KO mutant. The metabolites increased in *sir-2.1* are in red, those decreased in blue, and those without significant changes in black.

the various catabolic pathways and ATP generation. This may be also responsible for the higher GSSG level, as reactive oxygen species can be generated when oxidative phosphorylation is decoupled from catabolism. Overall, the decoupling between the enhanced catabolism and ATP generation may be a key metabotype of the *sir-2.1* mutant.

These metabotypes should help us understand the roles of *sir-2.1*, especially in relation to lifespan. The *sir-2.1* overexpression leads to moderate lifespan increase,[11,12] whereas its deletion leads to slight decrease.[37] In addition, the KO strain can live in apparently normal fashion (http://www.wormbase.org), despite the prevalent embryonic lethality of SIRT1 KO mice.[38] Therefore, *sir-2.1* seems to have relatively small effects on readily identifiable external phenotypes. Still, our sensitive metabolomics approach using *in vivo* labeling allowed us to characterize the metabotypes at individual metabolite levels. Importantly, the small degree of lifespan changes by *sir-2.1* seems to agree well with the modest changes in the levels of BCAAs with high statistical significance ($p \approx 10^{-5}$ or lower).

The BCAAs deserve further discussion, as they recently gathered much attention in relation to lifespan. In diverse model systems, such as yeasts,[39] mice,[40] and *C. elegans*,[18] BCAAs have been implicated in longer life span and/or mitochondrial biogenesis.[41] In yeasts, they were shown to increase the chronological lifespan by suppressing GCN4, a key regulator of general amino acid control pathway,[42] and their reduced levels decreased the chronological lifespan.[39] In *C. elegans*, the *daf-2* mutant exhibited increased levels of BCAAs and glutamine, and decreased levels of choline, betaine, and glutamate.[18] Very interestingly, the changes in all of these seven metabolites are exactly the opposite to those observed in our *sir-2.1* mutant. Considering the *daf-2* mutant's longer and *sir-2.1* mutant's slightly shorter lifespan,[37] these opposite directions are consistent with the mutation's effects on the lifespan and corroborate our results. In higher rodent system, BCAAs were shown to induce mitochondrial biogenesis and SIRT1 expression in cardiac and skeletal muscle and to increase their average lifespan.[40] It was suggested that BCAAs reduce the ROS generation in mitochondria through eNOS activity that may have mutual feedback with the mTOR pathway. The decreased ROS levels by supplementation of BCAAs in the mouse system are in line with our finding that *sir-2.1* deletion leads to decreased BCAA and increased GSSG levels. Interestingly, the mouse study also suggested that BCAAs induce SIRT1 in cardiac and skeletal muscles, while our results showed that *sir-2.1* deficiency lowers the BCAA levels. It may be possible that BCAAs and *sir-2.1* have reciprocally positive effects on each other, just like the above-stated mutual feedback between mTOR and eNOS. Another possibility is that the BCAA levels and SIRT1 relationship is tissue-dependent, as shown in the mouse study, and our results reflect the tissue-averaged effects, as we used the whole organism. Collectively our and previous works highlight the roles of BCAAs and their relationship with SIRT1 in the determination of lifespans of model organisms.

Here, we applied *in vivo* ^{13}C-labeling optimized for multidimensional NMR metabolomics to characterize the metabotypes of *C. elegans sir-2.1* mutant. We successfully defined the metabotype as decoupling between various catabolic pathways and ATP generation. We also suggested the relationship between the metabotypes, especially the BCAA levels, and the roles of *sir-2.1* in the worm lifespan. These suggest that the metabotype characterization is very sensitive and can provide valuable insights into protein functions, even when apparent phenotypic changes are only modest. As *C. elegans* is widely used in metabolism and lifespan studies, our approach is expected to help understand many other protein functions in metabolic perspectives.

METHODS

Preparation of ^{13}C-Labeled *E. coli*. NaCl (1.5 g), agar (10 g), and uracil (1.14 g) were dissolved in 484 mL of distilled water, and the mixture was autoclaved. Uracil was added, as the *E. coli* strain (OP50 strain) is a uracil auxotroph. One gram of $^{13}C_6$-glucose, 1 g of NH_4Cl, 0.5 mL of 1 M $CaCl_2$, 0.5 mL of 1 M $MgSO_4$, 0.5 mL of 1% (v/v) thiamine, 2 mL of cholesterol (5 mg mL^{-1}), and 12.5 mL of 1 M KH_2PO_4 (pH 6.0) buffer were additionally added to the mixture. The agar solution was poured into 100 mm plastic Petri dish plates.

The *E. coli* (OP50 strain) was initially grown at 37 °C overnight in liquid M9 media (500 mL) composed of NaH_2PO_4 (3.4 g), K_2HPO_4 (1.5 g), NaCl (0.25 g), and uracil (1.19 g) and a filtered mixture containing $^{13}C_6$-glucose (1 g), NH_4Cl (1 g), 1 M $CaCl_2$ (50 μL), 1 M $MgSO_4$ (0.5 mL), 1% (v/v) thiamine (0.5 mL), and streptomycin (X1000, 500 μL). The cultured *E. coli* was harvested with centrifugation at 1,910*g* for 5 min at RT, and the pellet was resuspended in 50 mL of culture media. One milliliter of this *E. coli* suspension was spread on to one agar plate, and the plate was incubated at 37 °C overnight. For unlabeled samples, all of the procedures were the same as mentioned above, except for using $^{12}C_6$-glucose instead of $^{13}C_6$-glucose.

***C. elegans* Culture and Metabolite Extraction.** Wild type *C. elegans* Bristol strain (N2) was used, and the VC199 (*sir-2.1* (ok434) IV) strain was obtained from Dr. Jungho Kim at Inha university (Incheon, Korea). The worms were cultured on stable isotope labeling plates (see above) at 20 °C. All strains were synchronized, and the eggs were inoculated onto agar plates and grown up to young adult stage. The individual plate was washed with 8 mL of M9 buffer, and the worms were harvested at 100*g* for 1 min at RT, after which the pellets were washed with distilled water twice. The whole animals were lyzed with a tissue lyser bead mill (Biospec) in 2:1 methanol/chloroform mixture (600 μL) by vortexing for 45 s and incubation on ice for 15 s. This lysis step was repeated for five times. The lysate was

dx.doi.org/10.1021/cb3004226 | *ACS Chem. Biol.* 2012, 7, 2012–2018

sonicated for 15 min in cold water, and 1:1 chloroform/water mixture (400 μL) was added. The solution was then centrifuged at 15,000*g* for 20 min at 4 °C. The upper water phase and lower organic solvent phase were collected separately and dried with a centrifugal evaporator (Vision). The resulting extracts were stored at −20 °C until analysis.

NMR Experiments and Statistical Analysis. The dried upper water phase was dissolved with 450 μL of D_2O buffer containing 100 mM potassium phosphate (pH 7.0) and 1 mM 4,4-dimethyl-4-silapentane-1-sulfonic acid as internal standard. The organic layer samples were dissolved in 450 μL of deuterated chloroform. 2D and 3D NMR was performed on the aqueous phase, as it contains the vast majority of important metabolites. For the organic phase, 1D NMR data were obtained for average triacylglycerol and fatty acids level assessment. The dissolved samples were transferred into a 5 mm NMR tube. The HSQC, HMBC, and HCCH-TOCSY NMR spectra were obtained using a 900 MHz Bruker Avance spectrometer equipped with a cryogenic triple resonance probe at the Korea Basic Science Institute (Ochang, Korea) supported by the Bio-MR Research Program of the Korean Ministry of Science and Technology (E29070). All multi-dimensional spectra were analyzed with nmrview software (One moon Scientific). The processing and analysis of the 2D HSQC spectra to extract quantitative information was performed similarly to those reported previously[43,44] with some modifications. The integrated peak volumes, instead of the binned grid, of the 2D HSQC spectra were normalized against the total peak volumes and then used for the statistical analysis. Among the several peaks for a particular metabolites, the least overlapped peak was chosen for quantitation. Metabolite identification was performed by HSQC, HMBC, HCCH-TOCSY analysis along with in-house and public databases.[27] Origin (Originlab), SIMCA-P 11.0 (Umetrics), and in-house Perl script were used for statistical analysis. For orthogonal projections to latent structures-discriminant analysis (OPLS-DA), class discrimination models were built until the cross-validated predictability value did not meaningfully increase to avoid overfitting of the statistical model.

LC−MS Analysis. For ATP, AMP, and GSSG quantitation, an API 2000 Mass Spectrometer (AB/SCIEX) equipped with an electrospray ionization (ESI) source was used in negative ion mode with −4.5 kV ion spray voltage and 300 °C heater (turbo) gas temperature. Multiple reaction monitoring(MRM) was setup using standard compounds and performed for individual extract. The chromatography part was performed with 1 μL of the sample injected into an HPLC (Agilent 1100 Series, Agilent, CO). Mobile phases were 10 mM ammonium carbonate (pH 9.1) in DW (A) and acetonitrile (B), and the flow rate was 0.15 mL min^{-1}. The gradient scheme was as follows: 80% B at 0 min, 35% B at 10 min, 5% B at 12 min, 5% B at 25 min, 80% B at 25.1 min, and 80% B at 35 min. A Zic-Philic Polymeric Beads Peek Column (150 mm × 2.1 mm, 5 μm, Merck kGaA) was used at 35 °C, and autosampler temperature was set at 4 °C. For isotopic composition analysis and acetyl-CoA measurement, an LTQ XL high performance linear ion trap mass spectrometer (Thermo Fisher Scientific Inc., Waltham) equipped with an electrospray ionization (ESI) source (300 °C capillary temperature and 4 kV ion spray voltage) was used. The HPLC, column, mobile phases, and operation temperature were the same as above. The flow rate was 0.1 mL min^{-1}, and the gradient was as follows: 80% B at 0 min, 20% B at 30 min, 20% B at 45 min, 80% B at 45.1 min, and 80% B at 60 min.

■ ASSOCIATED CONTENT

Supporting Information

Isotopic enrichment measurement data by LC−MS, a zoomed region of 2D HSQC NMR spectrum, metabolite assignment table, principal component analysis (PCA) of WT and *sir-2.1* samples, LC−MS quantitation of metabolites, and comparison of the difference HSQC spectra between WT and *sir-2.1* mutant. This material is available free of charge *via* the Internet at http://pubs.acs.org.

■ AUTHOR INFORMATION

Corresponding Author

*E-mail: psh@snu.ac.kr.

Notes

The authors declare no competing financial interest.

■ ACKNOWLEDGMENTS

This study was supported by grants from the National R&D Program for Cancer Control, Ministry of Health & Welfare, Korea (1120300), and from the National Research Foundation of Korea (NRF) funded by the Ministry of Education, Science and Technology, Korea (2012011362 and 20110030635 to S.P., and 2010-0026035 to J.L.). This study was also supported by a grant from the Korea Healthcare Technology R&D Project, Ministry for Health and Wealfare, Republic of Korea to S.P. (A092006).

■ ABBREVIATIONS

BCAA, branched chain amino acids; OPLS-DA, orthogonal projections to latent structures-discriminant analysis; MRM, multiple reaction monitoring; HMN, heteronuclear multi-dimensional NMR

■ REFERENCES

(1) Kaeberlein, M., McVey, M., and Guarente, L. (1999) The SIR2/3/4 complex and SIR2 alone promote longevity in Saccharomyces cerevisiae by two different mechanisms. *Genes Dev. 13*, 2570−2580.

(2) Tissenbaum, H. A., and Guarente, L. (2001) Increased dosage of a sir-2 gene extends lifespan in *Caenorhabditis elegans*. *Nature 410*, 227−230.

(3) Rogina, B., and Helfand, S. L. (2004) Sir2 mediates longevity in the fly through a pathway related to calorie restriction. *Proc. Natl. Acad. Sci. U.S.A. 101*, 15998−16003.

(4) Kanfi, Y., Naiman, S., Amir, G., Peshti, V., Zinman, G., Nahum, L., Bar-Joseph, Z., and Cohen, H. Y. (2012) The sirtuin SIRT6 regulates lifespan in male mice. *Nature 483*, 218−221.

(5) Herranz, D., and Serrano, M. (2010) SIRT1: recent lessons from mouse models. *Nat. Rev. Cancer 10*, 819−823.

(6) Guarente, L. (2011) Sirtuins, aging, and medicine. *N. Engl. J. Med. 364*, 2235−2244.

(7) Baur, J. A., Ungvari, Z., Minor, R. K., Le Couteur, D. G., and de Cabo, R. (2012) Are sirtuins viable targets for improving healthspan and lifespan? *Nat. Rev. Drug Discovery 11*, 443−461.

(8) Milne, J. C., Lambert, P. D., Schenk, S., Carney, D. P., Smith, J. J., Gagne, D. J., Jin, L., Boss, O., Perni, R. B., Vu, C. B., Bemis, J. E., Xie, R., Disch, J. S., Ng, P. Y., Nunes, J. J., Lynch, A. V., Yang, H., Galonek, H., Israelian, K., Choy, W., Iffland, A., Lavu, S., Medvedik, O., Sinclair, D. A., Olefsky, J. M., Jirousek, M. R., Elliott, P. J., and Westphal, C. H. (2007) Small molecule activators of SIRT1 as therapeutics for the treatment of type 2 diabetes. *Nature 450*, 712−716.

(9) Herranz, D., Munoz-Martin, M., Canamero, M., Mulero, F., Martinez-Pastor, B., Fernandez-Capetillo, O., and Serrano, M. (2010) Sirt1 improves healthy ageing and protects from metabolic syndrome-associated cancer. *Nat. Commun. 1*, 3.

(10) Burnett, C., Valentini, S., Cabreiro, F., Goss, M., Somogyvari, M., Piper, M. D., Hoddinott, M., Sutphin, G. L., Leko, V., McElwee, J. J., Vazquez-Manrique, R. P., Orfila, A. M., Ackerman, D., Au, C., Vinti, G., Riesen, M., Howard, K., Neri, C., Bedalov, A., Kaeberlein, M., Soti, C., Partridge, L., and Gems, D. (2011) Absence of effects of Sir2 overexpression on lifespan in *C. elegans* and *Drosophila*. *Nature 477*, 482−485.

(11) Rizki, G., Iwata, T. N., Li, J., Riedel, C. G., Picard, C. L., Jan, M., Murphy, C. T., and Lee, S. S. (2011) The evolutionarily conserved longevity determinants HCF-1 and SIR-2.1/SIRT1 collaborate to regulate DAF-16/FOXO. *PLoS Genet. 7*, e1002235.

(12) Viswanathan, M., and Guarente, L. (2011) Regulation of Caenorhabditis elegans lifespan by sir-2.1 transgenes. *Nature 477*, E1−2.
(13) Pacholec, M., Bleasdale, J. E., Chrunyk, B., Cunningham, D., Flynn, D., Garofalo, R. S., Griffith, D., Griffor, M., Loulakis, P., Pabst, B., Qiu, X., Stockman, B., Thanabal, V., Varghese, A., Ward, J., Withka, J., and Ahn, K. (2010) SRT1720, SRT2183, SRT1460, and resveratrol are not direct activators of SIRT1. *J. Biol. Chem. 285*, 8340−8351.
(14) Dai, H., Kustigian, L., Carney, D., Case, A., Considine, T., Hubbard, B. P., Perni, R. B., Riera, T. V., Szczepankiewicz, B., Vlasuk, G. P., and Stein, R. L. (2010) SIRT1 activation by small molecules: kinetic and biophysical evidence for direct interaction of enzyme and activator. *J. Biol. Chem. 285*, 32695−32703.
(15) Kaeberlein, M., McDonagh, T., Heltweg, B., Hixon, J., Westman, E. A., Caldwell, S. D., Napper, A., Curtis, R., DiStefano, P. S., Fields, S., Bedalov, A., and Kennedy, B. K. (2005) Substrate-specific activation of sirtuins by resveratrol. *J. Biol. Chem. 280*, 17038−17045.
(16) Patti, G. J., Yanes, O., and Siuzdak, G. (2012) Metabolomics: the apogee of the omics trilogy. *Nat. Rev. Mol. Cell Biol. 13*, 263−269.
(17) Fuchs, S., Bundy, J., Davies, S., Viney, J., Swire, J., and Leroi, A. (2010) A metabolic signature of long life in *Caenorhabditis elegans*. *BMC Biol. 8*, 14.
(18) Martin, F. P., Spanier, B., Collino, S., Montoliu, I., Kolmeder, C., Giesbertz, P., Affolter, M., Kussmann, M., Daniel, H., Kochhar, S., and Rezzi, S. (2011) Metabotyping of *Caenorhabditis elegans* and their culture media revealed unique metabolic phenotypes associated to amino acid deficiency and insulin-like signaling. *J. Proteome Res. 10*, 990−1003.
(19) Hughes, S. L., Bundy, J. G., Want, E. J., Kille, P., and Stürzenbaum, S. R. (2009) The metabolomic responses of *Caenorhabditis elegans* to cadmium are largely independent of metallothionein status, but dominated by changes in cystathionine and phytochelatins. *J. Proteome Res. 8*, 3512−3519.
(20) Lewis, I. A., Schommer, S. C., Hodis, B., Robb, K. A., Tonelli, M., Westler, W. M., Sussman, M. R., and Markley, J. L. (2007) Method for determining molar concentrations of metabolites in complex solutions from two-dimensional 1H-13C NMR spectra. *Anal. Chem. 79*, 9385−9390.
(21) Forseth, R. R., Fox, E. M., Chung, D., Howlett, B. J., Keller, N. P., and Schroeder, F. C. (2011) Identification of cryptic products of the gliotoxin gene cluster using NMR-based comparative metabolomics and a model for gliotoxin biosynthesis. *J. Am. Chem. Soc. 133*, 9678−9681.
(22) Pungaliya, C., Srinivasan, J., Fox, B. W., Malik, R. U., Ludewig, A. H., Sternberg, P. W., and Schroeder, F. C. (2009) A shortcut to identifying small molecule signals that regulate behavior and development in *Caenorhabditis elegans*. *Proc. Natl. Acad. Sci. U.S.A. 106*, 7708−7713.
(23) Robinette, S. L., Ajredini, R., Rasheed, H., Zeinomar, A., Schroeder, F. C., Dossey, A. T., and Edison, A. S. (2011) Hierarchical alignment and full resolution pattern recognition of 2D NMR spectra: application to nematode chemical ecology. *Anal. Chem. 83*, 1649−1657.
(24) Sekiyama, Y., Chikayama, E., and Kikuchi, J. (2011) Evaluation of a semipolar solvent system as a step toward heteronuclear multidimensional NMR-based metabolomics for 13C-labeled bacteria, plants, and animals. *Anal. Chem. 83*, 719−726.
(25) Chikayama, E., Suto, M., Nishihara, T., Shinozaki, K., Hirayama, T., and Kikuchi, J. (2008) Systematic NMR analysis of stable isotope labeled metabolite mixtures in plant and animal systems: coarse grained views of metabolic pathways. *PloS One 3*, e3805.
(26) Kikuchi, J., Shinozaki, K., and Hirayama, T. (2004) Stable isotope labeling of *Arabidopsis thaliana* for an NMR-based metabolomics approach. *Plant. Cell Physiol. 45*, 1099−1104.
(27) Chikayama, E., Sekiyama, Y., Okamoto, M., Nakanishi, Y., Tsuboi, Y., Akiyama, K., Saito, K., Shinozaki, K., and Kikuchi, J. (2010) Statistical indices for simultaneous large-scale metabolite detections for a single NMR spectrum. *Anal. Chem. 82*, 1653−1658.
(28) Xia, J., Bjorndahl, T. C., Tang, P., and Wishart, D. S. (2008) MetaboMiner—semi-automated identification of metabolites from 2D NMR spectra of complex biofluids. *BMC Bioinformatics 9*, 507.
(29) Perez, C. L., and Van Gilst, M. R. (2008) A 13C isotope labeling strategy reveals the influence of insulin signaling on lipogenesis in *C. elegans*. *Cell Metab. 8*, 266−274.
(30) Gouw, J. W., Tops, B. B., and Krijgsveld, J. (2011) Metabolic labeling of model organisms using heavy nitrogen (15N). *Methods Mol. Biol. 753*, 29−42.
(31) Larance, M., Bailly, A. P., Pourkarimi, E., Hay, R. T., Buchanan, G., Coulthurst, S., Xirodimas, D. P., Gartner, A., and Lamond, A. I. (2011) Stable-isotope labeling with amino acids in nematodes. *Nat. Methods 8*, 849−851.
(32) Fredens, J., Engholm-Keller, K., Giessing, A., Pultz, D., Larsen, M. R., Hojrup, P., Moller-Jensen, J., and Faergeman, N. J. (2011) Quantitative proteomics by amino acid labeling in *C. elegans*. *Nat. Methods 8*, 845−847.
(33) Castro, C., Sar, F., Shaw, W. R., Mishima, M., Miska, E. A., and Griffin, J. L. (2012) A metabolomic strategy defines the regulation of lipid content and global metabolism by Δ9 desaturases in *Caenorhabditis elegans*. *BMC Genomics 13*, 36.
(34) Hallows, W. C., Yu, W., and Denu, J. M. (2012) Regulation of glycolytic enzyme phosphoglycerate mutase-1 by Sirt1 protein-mediated deacetylation. *J. Biol. Chem. 287*, 3850−3858.
(35) Gottlieb, E., and Vousden, K. H. (2010) p53 regulation of metabolic pathways. *Cold Spring Harbor Perspect. Biol. 2*, a001040.
(36) Indiveri, C., Iacobazzi, V., Tonazzi, A., Giangregorio, N., Infantino, V., Convertini, P., Console, L., and Palmieri, F. (2011) The mitochondrial carnitine/acylcarnitine carrier: function, structure and physiopathology. *Mol. Aspects Med. 32*, 223−233.
(37) Wang, Y., and Tissenbaum, H. A. (2006) Overlapping and distinct functions for a *Caenorhabditis elegans* SIR2 and DAF-16/FOX. *Mech. Ageing Dev. 127*, 48−56.
(38) Wang, R. H., Sengupta, K., Li, C., Kim, H. S., Cao, L., Xiao, C., Kim, S., Xu, X., Zheng, Y., Chilton, B., Jia, R., Zheng, Z. M., Appella, E., Wang, X. W., Ried, T., and Deng, C. X. (2008) Impaired DNA damage response, genome instability, and tumorigenesis in SIRT1 mutant mice. *Cancer Cell 14*, 312−323.
(39) Alvers, A. L., Fishwick, L. K., Wood, M. S., Hu, D., Chung, H. S., Dunn, W. A., Jr., and Aris, J. P. (2009) Autophagy and amino acid homeostasis are required for chronological longevity in *Saccharomyces cerevisiae*. *Aging Cell 8*, 353−369.
(40) D'Antona, G., Ragni, M., Cardile, A., Tedesco, L., Dossena, M., Bruttini, F., Caliaro, F., Corsetti, G., Bottinelli, R., Carruba, M. O., Valerio, A., and Nisoli, E. (2010) Branched-chain amino acid supplementation promotes survival and supports cardiac and skeletal muscle mitochondrial biogenesis in middle-aged mice. *Cell Metab. 12*, 362−372.
(41) Valerio, A., D'Antona, G., and Nisoli, E. (2011) Branched-chain amino acids, mitochondrial biogenesis, and healthspan: an evolutionary perspective. *Aging 3*, 464−478.
(42) Hinnebusch, A. G. (2005) Translational regulation of GCN4 and the general amino acid control of yeast. *Annu. Rev. Microbiol. 59*, 407−450.
(43) Sekiyama, Y., Chikayama, E., and Kikuchi, J. (2010) Profiling polar and semipolar plant metabolites throughout extraction processes using a combined solution-state and high-resolution magic angle spinning NMR approach. *Anal. Chem. 82*, 1643−1652.
(44) Nakanishi, Y., Fukuda, S., Chikayama, E., Kimura, Y., Ohno, H., and Kikuchi, J. (2011) Dynamic omics approach identifies nutrition-mediated microbial interactions. *J. Proteome Res. 10*, 824−836.